

Science

 AAAS

Plant Immunity Requires Conformational Charges of NPR1 via S-Nitrosylation and Thioredoxins

Yasuomi Tada, *et al.*

Science **321**, 952 (2008);

DOI: 10.1126/science.1156970

The following resources related to this article are available online at www.sciencemag.org (this information is current as of August 15, 2008):

Updated information and services, including high-resolution figures, can be found in the online version of this article at:

<http://www.sciencemag.org/cgi/content/full/321/5891/952>

Supporting Online Material can be found at:

<http://www.sciencemag.org/cgi/content/full/1156970/DC1>

This article **cites 24 articles**, 13 of which can be accessed for free:

<http://www.sciencemag.org/cgi/content/full/321/5891/952#otherarticles>

This article appears in the following **subject collections**:

Botany

<http://www.sciencemag.org/cgi/collection/botany>

Information about obtaining **reprints** of this article or about obtaining **permission to reproduce this article** in whole or in part can be found at:

<http://www.sciencemag.org/about/permissions.dtl>

conditions were more common, and that episodes of deep-water oxygenation preceded the Gaskiers or even earlier glaciations. Future work should resolve this.

In the modern world, and through much of the Phanerozoic Eon (19), marine anoxia produces sulfidic conditions. Why was this not generally true in the later Neoproterozoic? The persistence of Fe in anoxic deep waters requires that the molar flux of FeHR to the deep ocean be greater than half the flux of sulfide, the ratio needed to give excess Fe after the formation of FeS₂ (3). Therefore, to explain Neoproterozoic ferruginous deep-water chemistry, we must appeal to factors that either limited S input to the ocean or increased the input of Fe. Indeed, both may have been in play. Previous modeling has suggested that the surface inventory of S may have decreased in size through the Mesoproterozoic and into the Neoproterozoic because of the subduction of sedimentary sulfides deposited beneath sulfidic ocean waters (32). This would have made less S available for weathering and reduced the flux of sulfate to the ocean. Furthermore, Neoproterozoic sulfate concentrations were probably much less than today (32, 33). Reduced sulfate levels change the redox balance during mid-ocean ridge hydrothermal circulation, resulting in an increased flux of Fe from hydrothermal fluids to the oceans (34). We propose that these processes, either singly or combined, produced the chemistry of later Neoproterozoic oceans.

References and Notes

- H. D. Holland, *The Chemical Evolution of the Atmosphere and Oceans* (Princeton Univ. Press, Princeton, NJ, 1982).
- D. E. Canfield, K. S. Habicht, B. Thamdrup, *Science* **288**, 658 (2000).
- D. E. Canfield, *Nature* **396**, 450 (1998).
- C. Scott *et al.*, *Nature* **452**, 456 (2008).
- Y. Shen, A. H. Knoll, M. R. Walter, *Nature* **423**, 632 (2003).
- S. W. Poulton, P. W. Fralick, D. E. Canfield, *Nature* **431**, 173 (2004).
- H. D. Holland, *Philos. Trans. R. Soc. London Ser. B* **361**, 903 (2006).
- A. H. Knoll, S. B. Carrol, *Science* **284**, 2129 (1999).
- P. F. Hoffman, *S. Afr. J. Geol.* **108**, 557 (2005).
- J. L. Kirschvink, *Am. Assoc. Pet. Geol. Bull.* **75**, 610 (1991).
- P. F. Hoffman, A. J. Kaufman, G. P. Halverson, D. P. Schrag, *Science* **281**, 1342 (1998).
- D. E. Canfield, S. W. Poulton, G. M. Narbonne, *Science* **315**, 92 (2007).
- S. W. Poulton, D. E. Canfield, *Chem. Geol.* **214**, 209 (2005).
- R. Raiswell, D. E. Canfield, *Am. J. Sci.* **298**, 219 (1998).
- Materials and methods are available as supporting material on Science Online.
- We have tried to avoid weathering by collecting in the field the freshest material possible, and furthermore, we have removed any further evidence of weathering when preparing samples for crushing, powdering, and eventual chemical extraction. Still, oxidative weathering is possible in some cases. The main influence of weathering will be to oxidize reduced-Fe phases such as FeS₂ and Fe carbonates to Fe oxides. In this way, the total reactive Fe content of the sample would be little affected, although the distribution of phases might be. For this reason, some of our FeS₂ and Fe carbonate contents may be underestimated. This is probably the worst for our Sheepbed samples, although all of these still retain FeS₂, sometimes in appreciable amounts (15). Nonetheless, even if we underestimate the FeS₂ and Fe carbonate contents of some samples because of weathering, our evaluation of the nature of ocean chemistry, and particularly the dominance of ferruginous conditions, is generally not affected. This is because although some Fe carbonate may have been lost, the Fe carbonate contents of most samples are high enough to preclude deposition in a sulfidic water column—even making the extreme (and probably incorrect) assumption that all Fe oxides represent oxidized FeS₂.
- D. Z. Oehler, J. H. Oehler, A. J. Stewart, *Science* **205**, 388 (1979).
- J. W. Green, A. H. Knoll, K. Swett, *Geol. Mag.* **126**, 567 (1989).
- S. W. Poulton, R. Raiswell, *Am. J. Sci.* **302**, 774 (2002).
- K. K. Turekian, K. H. Wedepohl, *Geol. Soc. Am. Bull.* **72**, 175 (1961).
- T. W. Lyons, S. Severmann, *Geochim. Cosmochim. Acta* **70**, 5698 (2006).
- G. M. Ross, J. D. Bloch, H. R. Krouse, *Precambrian Res.* **73**, 71 (1995).
- D. A. Fike, J. P. Grotzinger, L. M. Pratt, R. E. Summons, *Nature* **444**, 744 (2006).
- K. A. McFadden *et al.*, *Proc. Natl. Acad. Sci. U.S.A.* **105**, 3197 (2008).
- Y. Shen, T. Zhang, P. F. Hoffman, *Proc. Natl. Acad. Sci. U.S.A.* **105**, 7376 (2008).
- C. M. Dehler *et al.*, *Sediment. Geol.* **141**, 465 (2001).
- K. E. Karlstrom *et al.*, *Geology* **28**, 619 (2000).
- T. Goldberg, H. Strauss, Q. Guo, C. Liu, *Palaeogeogr. Palaeoclimatol. Palaeoecol.* **254**, 175 (2007).
- B. Lehmann *et al.*, *Geology* **35**, 403 (2007).
- H. Kimura, Y. Watanabe, *Geology* **29**, 995 (2001).
- S. Schroder, J. P. Grotzinger, *J. Geol. Soc. London* **164**, 175 (2007).
- D. E. Canfield, *Am. J. Sci.* **304**, 839 (2004).
- L. C. Kah, T. W. Lyons, T. D. Frank, *Nature* **431**, 834 (2004).
- L. R. Kump, W. E. Seyfried Jr., *Earth Planet. Sci. Lett.* **235**, 654 (2005).
- For financial support, we thank Danmarks Grundforskningsfond, the Natural Environment Research Council (research fellowship to S.W.P.), NSF (Division of Earth Sciences grant 0420592 to A.H.K.), and the Natural Sciences and Engineering Research Council of Canada Discovery Grant, Northwest Territories Scientist's License. We acknowledge the help of N. P. James and T. K. Kyser; the insightful comments of D. Johnston; and the expert technical assistance of L. Salling, M. Andersen, and E. Hammarlund.

Supporting Online Material

www.sciencemag.org/cgi/content/full/1154499/DC1

Materials and Methods

Figs. S1 and S2

Table S1

References

21 December 2007; accepted 2 July 2008

Published online 17 July 2008;

10.1126/science.1154499

Include this information when citing this paper.

Plant Immunity Requires Conformational Changes of NPR1 via S-Nitrosylation and Thioredoxins

Yasuomi Tada,¹ Steven H. Spoel,¹ Karolina Pajeroska-Mukhtar,¹ Zhonglin Mou,^{1,*} Junqi Song,¹ Chun Wang,² Jianru Zuo,² Xinnian Dong^{1,†}

Changes in redox status have been observed during immune responses in different organisms, but the associated signaling mechanisms are poorly understood. In plants, these redox changes regulate the conformation of NPR1, a master regulator of salicylic acid (SA)-mediated defense genes. NPR1 is sequestered in the cytoplasm as an oligomer through intermolecular disulfide bonds. We report that S-nitrosylation of NPR1 by S-nitrosoglutathione (GSNO) at cysteine-156 facilitates its oligomerization, which maintains protein homeostasis upon SA induction. Conversely, the SA-induced NPR1 oligomer-to-monomer reaction is catalyzed by thioredoxins (TRXs). Mutations in both NPR1 cysteine-156 and TRX compromised NPR1-mediated disease resistance. Thus, the regulation of NPR1 is through the opposing action of GSNO and TRX. These findings suggest a link between pathogen-triggered redox changes and gene regulation in plant immunity.

Innate immune responses are evolutionarily conserved among plants and animals (1, 2) and are often associated with changes in cellular oxidative and reductive states. In plants, these

redox changes are sensed by the NPR1 protein, a master regulator of defense gene expression (3). In unchallenged plants, NPR1 resides in the cytoplasm as an oligomer maintained through

redox-sensitive intermolecular disulfide bonds. Upon pathogen challenge, the plant defense signaling molecule salicylic acid (SA) increases and changes the cellular redox state, leading to reduction of the disulfide bonds in NPR1. Reduction of the NPR1 oligomer releases monomer that translocates to the nucleus where it activates the expression of a battery of *pathogenesis-related* (PR) genes (4). Mutations at residues Cys⁸² and Cys²¹⁶ in NPR1 result in increased monomer accumulation, constitutive nuclear localization, and NPR1-mediated gene expression in the absence of pathogen challenge (3). On the basis of these results, it has been proposed that conformational changes in NPR1 (that is, oligomer-monomer exchange) regulate its nuclear translocation and activity (3).

Oligomerization of proteins through intermolecular disulfide bonds is unusual under reductive cytosolic conditions (5). However, treatment with SA not only induced NPR1 monomer release but also facilitated oligomerization in wild-type plants (fig. S1A). Similar results were obtained with biologically active NPR1 fused with green fluorescent protein (NPR1-GFP) (4) or with tandem affinity purification tag (NPR1-TAP) (fig.

S2), driven by the constitutive 35S promoter (Fig. 1A). On the basis of these observations, we hypothesized that a catalyst of cysteine thiol oxidation was involved in the formation of the NPR1 oligomer. To search for cellular oxidants facilitating NPR1 oligomerization, we established a cell-free assay in which total protein extract from 35S::NPR1-GFP plants was treated with the reducing agent dithiothreitol (DTT) to partially convert the NPR1-GFP oligomer to monomer. Removal of DTT by dialysis allowed reformation of the oligomer as shown by a decrease in monomer, while the total protein amount remained constant (Fig. 1B). These data suggest that, depending on the cellular environment, NPR1 switches between the oligomeric and monomeric states.

Using the cell-free assay shown in Fig. 1B, we tested the effect of hydrogen peroxide (H₂O₂) as well as the nitric oxide (NO) donors sodium nitroprusside (SNP) and S-nitrosoglutathione (GSNO) on the NPR1 oligomer-monomer equilibrium, because these oxidants accumulate during innate immune responses (6, 7). The treatment of protein extracts with H₂O₂ and SNP had no effect on NPR1 conformation (Fig. 1C). In contrast, GSNO, a natural NO donor, markedly facilitated oligomerization of NPR1 as shown by

the disappearance of the monomer while total NPR1 levels remained unchanged (Fig. 1C). This is consistent with the finding that unlike SNP, the treatment of plant cell cultures with GSNO caused protein S-nitrosylation (8), a process in which NO is covalently attached to a reactive cysteine thiol to form an S-nitrosothiol (SNO) (9). To further confirm this specific effect of GSNO, NPR1 activity was monitored in the GSNO reductase knockout mutant *atgsnor1-3*, which displays increased S-nitrosylation activity (7). We found that SA-induced monomerization of the endogenous NPR1 (fig. S1B) and nuclear translocation of monomeric NPR1-GFP were inhibited (Fig. 1D). NPR1 oligomer accumulated to higher levels in the *atgsnor1-3* mutant as compared to the wild type (fig. S1B). Accordingly, SA-induced expression of the NPR1-dependent defense gene *PR-1* was also suppressed in *atgsnor1-3* plants (Fig. 1E). These data suggest that GSNO affects the conformation of NPR1 and consequently its activity in innate immunity.

In *Arabidopsis*, pathogen infection induces an increase in cellular SNO levels, and elevated SNO levels in *atgsnor1-3* are associated with enhanced susceptibility to disease (7). The effect of GSNO on NPR1 oligomerization, together with the fact that some of the cysteine residues in NPR1 are critical for oligomer formation (3), suggests that one or more NPR1 cysteine thiols are directly modified by GSNO. To test this, we examined whether NPR1 is S-nitrosylated in planta, using the biotin-switch method (10), which specifically detects S-nitrosylated proteins (11). Total protein was extracted from SA-treated wild-type and transgenic 35S::NPR1-GFP plants and then incubated with or without ascorbate,

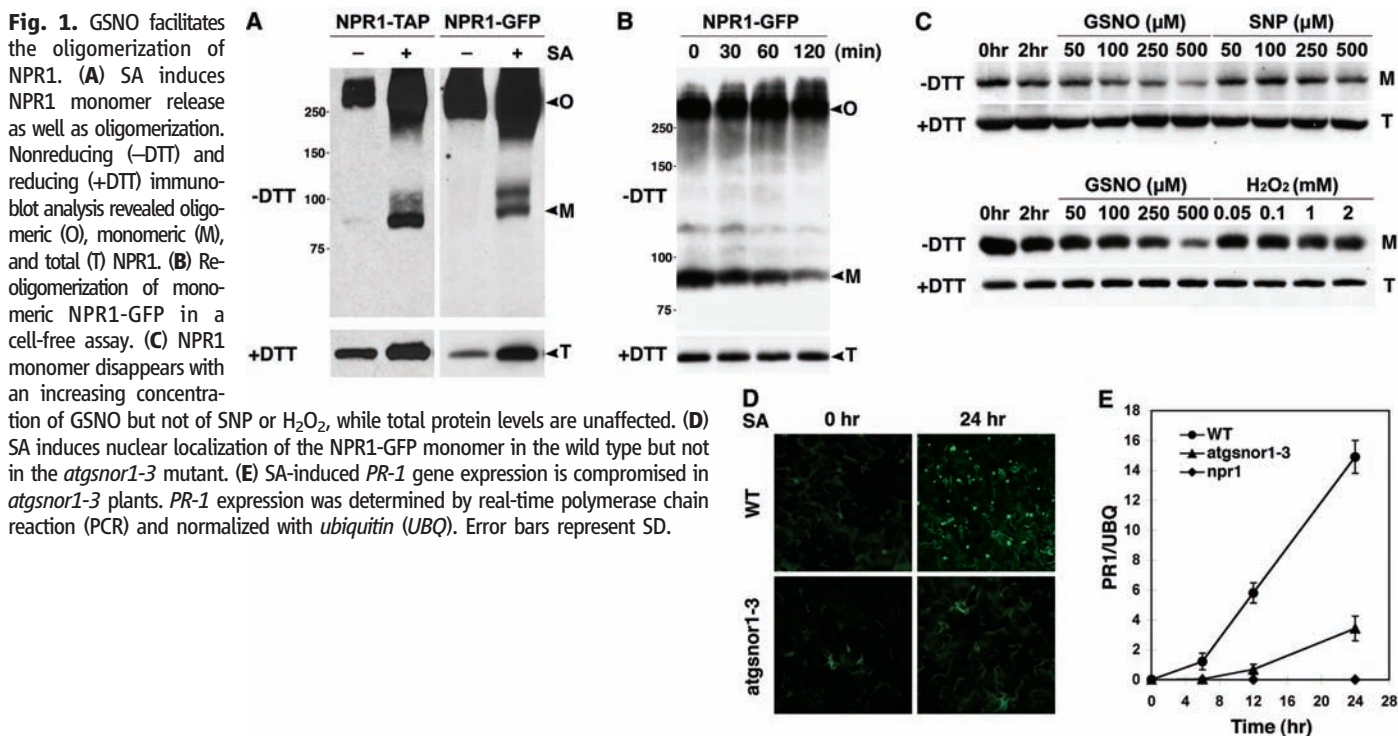
which specifically reduces SNO groups (10). The resulting free thiols were then covalently coupled to biotin-HPDP (biotin-N-[6(biotinamido)hexyl]-3'-(2'-pyridyldithio)propionamide) and immunoprecipitated with streptavidin beads. Immunoblot analysis revealed that both endogenous NPR1 and transgenic NPR1-GFP were pulled down only in ascorbate-treated samples, indicating that these proteins were specifically S-nitrosylated in vivo (Fig. 2A). Treatment with SA enhanced the S-nitrosylation of NPR1 (fig. S3A). We then applied the biotin-switch method to our cell-free assay and found that GSNO increased S-nitrosylation of NPR1, whereas SNP was ineffective in this respect (Fig. 2B). These results suggest that GSNO may facilitate NPR1 oligomerization directly through thiol S-nitrosylation.

Previously, we demonstrated that Cys⁸², Cys¹⁵⁰, Cys¹⁵⁵, Cys¹⁶⁰, and Cys²¹⁶ in and adjacent to the BTB/POZ domain of NPR1 (fig. S4) are important in the oligomer-monomer exchange (3). This suggests that the N-terminal half of NPR1 is sufficient for oligomerization. We purified recombinant protein containing the hexa-histidine (6xHis)-tagged N-terminal half of NPR1 (His6-NH, residues 1 to 246) and examined its oligomerization properties in response to NO donors. As compared with the control, treatment of purified His6-NH with GSNO resulted in increased S-nitrosylation and multimerization of His6-NH (Fig. 2C). Similar results were obtained with the NO donor diethylamine-NO (DEA/NO) (fig. S3, B and C), further supporting a role of SNO in stimulating NPR1 oligomerization. In contrast, SNP treatment failed to S-nitrosylate and multimerize His6-NH (Fig. 2C). Thus, at least one NO-sensitive cysteine lies within the 246 N-terminal

¹Department of Biology, Post Office Box 90338, Duke University, Durham, NC 27708, USA. ²Institute of Genetics and Developmental Biology, Chinese Academy of Sciences, Beijing 100101, China.

*Present address: Department of Microbiology and Cell Science, Post Office Box 110700, University of Florida, Gainesville, FL 32611, USA.

†To whom correspondence should be addressed. E-mail: xdong@duke.edu



residues of NPR1. Indeed, mutation of Cys¹⁵⁶ abolished both GSNO-triggered S-nitrosylation (Fig. 2D) and oligomerization (Fig. 2E). Taken together, these findings indicate that GSNO S-nitrosylates NPR1 at Cys¹⁵⁶. Similar to the SNO-mediated disulfide bond formation in myoglobin (12, 13), S-nitrosylation of Cys¹⁵⁶ may directly facilitate disulfide linkage between NPR1 monomers. Computational modeling of the NPR1 BTB domain according to previously published BTB crystal structures (14, 15) predicts that one or more disulfide bonds may form between Cys¹⁵⁰, Cys¹⁵⁵, Cys¹⁵⁶, and Cys¹⁶⁰ in the NPR1 oligomer (fig. S5). Alternatively, S-nitrosylation of Cys¹⁵⁶ may lead to conformational changes in NPR1 that favor oligomerization as reported for SNO-facilitated dynamin oligomerization (16).

Transformation of *35S::NPR1C156A-GFP* into mutant *npr1* plants consistently resulted in constitutive nuclear fluorescence relative to uninduced *35S::NPR1-GFP* plants (Fig. 3A), suggesting that the NPR1C156A-GFP (C156A, Cys¹⁵⁶→Asp¹⁵⁶) protein does not form oligomers as efficiently as wild-type protein. Although NPR1C156A-GFP protein still formed oligomers before induction, it lacked any SA-induced increase in oligomerization (Fig. 3B), indicating that Cys¹⁵⁶ is required for SNO-facilitated oligomerization in vivo.

The effect of the *NPR1C156A* mutation on plant defense was demonstrated when plants were challenged by *Pseudomonas syringae* pv. *maculicola* ES4326 (*Psm* ES4326). Consistent with the nuclear accumulation of NPR1C156A-GFP (Fig. 3A) and its normal interaction with TGA transcription factors (fig. S6), untreated *35S::NPR1C156A-GFP* plants showed enhanced resistance to this pathogen as compared with *35S::NPR1-GFP* plants (Fig. 3C). However, unlike *35S::NPR1-GFP*, treatment with SA for 48 hours did not enhance resistance in *35S::NPR1C156A-GFP* plants. These findings indicate that SNO-Cys¹⁵⁶-mediated oligomerization is necessary to maintain NPR1 homeostasis upon SA activation. Immunoblot analysis (Fig. 3D) and GFP fluorescence (Fig. 3A) showed that the NPR1C156A protein was depleted 48 hours after SA treatment, explaining the compromised pathogen resistance.

To counter the effect of SNO-facilitated NPR1 oligomerization, reducing agents must be engaged upon SA induction to catalyze the NPR1 oligomer-to-monomer switch. To identify such agents, we performed pull-down assays with recombinant His6-NH protein and identified two thioredoxins (TRXs), TRX-h3 and TRX-h5 (Fig. 4A). Among the eight cytosolic *TRX-h* genes in *Arabidopsis*, *TRX-h5* is substantially up-regulated upon infection with *P. syringae* (17), whereas *TRX-h3* is the most highly constitutively expressed *TRX-h* (18) (fig. S7). In a reverse experiment, we covalently trapped NPR1 using mutant TRXs (TRX-h3M and TRX-h5M), in which the second catalytic cysteine was changed to serine to prevent the completion of substrate reduction

(19) (fig. S8A). Pull-down experiments showed that the NPR1-binding affinity of TRX-h was inversely correlated with its enzymatic activity (fig. S8, B and C), suggesting that TRX-h is the enzyme catalyzing NPR1 oligomer reduction. The transient nature of this interaction made it difficult

to examine the NPR1/TRX-h interaction in vivo. Therefore, we fixed the enzyme-substrate intermediate [see supporting online material (SOM) text] and coimmunoprecipitated TRX-5h with NPR1-TAP (Fig. 4B). Treatment with SA further increased the interaction. In vivo interaction of

Fig. 2. S-nitrosylation of Cys¹⁵⁶ facilitates the assembly of NPR1 oligomer. (A) SA induces S-nitrosylation of endogenous NPR1 and the NPR1-GFP proteins in vivo. Sodium ascorbate (Asc) was used to specifically detect S-nitrosylated (SNO) NPR1. Equal loading was verified with antibodies against NPR1 or NPR1-GFP. (B) GSNO, but not mock (–) or SNP treatment, induces S-nitrosylation of NPR1-GFP in plant extracts. S-nitrosylated NPR1-GFP was detected with the biotin-switch assay. An antibody against NPR1-GFP was used to verify equal loading. (C) GSNO, but not mock (–) or SNP treatment, induces S-nitrosylation and multimerization (black arrows) of recombinant His6-NH (NPR1 residues 1 to 246) monomer (gray arrow). Equal loading was verified with an antibody to NPR1. (D) Cys¹⁵⁶ is the principal site of S-nitrosylation in NPR1. Recombinant His6-NH and His6-NH-C156A proteins were incubated with different GSNO concentrations, and S-nitrosylation was detected by the biotin-switch assay. Equal loading was verified with an antibody to NPR1. (E) The C156A mutation impairs GSNO-induced oligomerization. Recombinant His6-NH and His6-NH-C156A proteins were treated with GSNO and with (+) or without (–) sodium ascorbate. Subsequently, monomers were allowed to re-oligomerize for the indicated times. Monomeric (–DTT) and total (+DTT) proteins were detected with an antibody to NPR1.

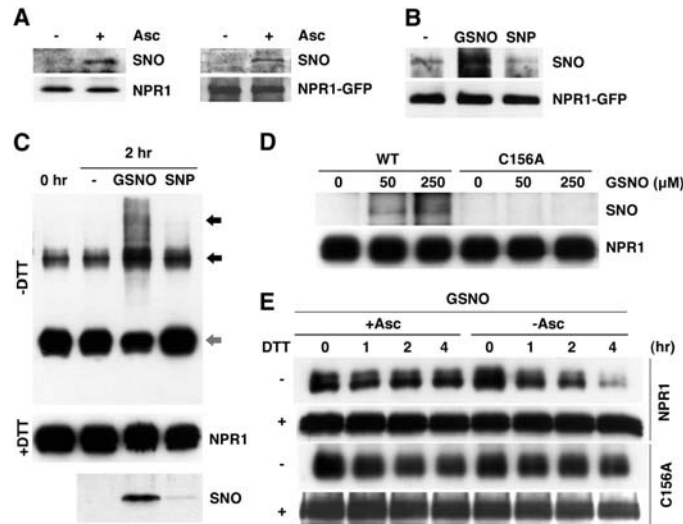
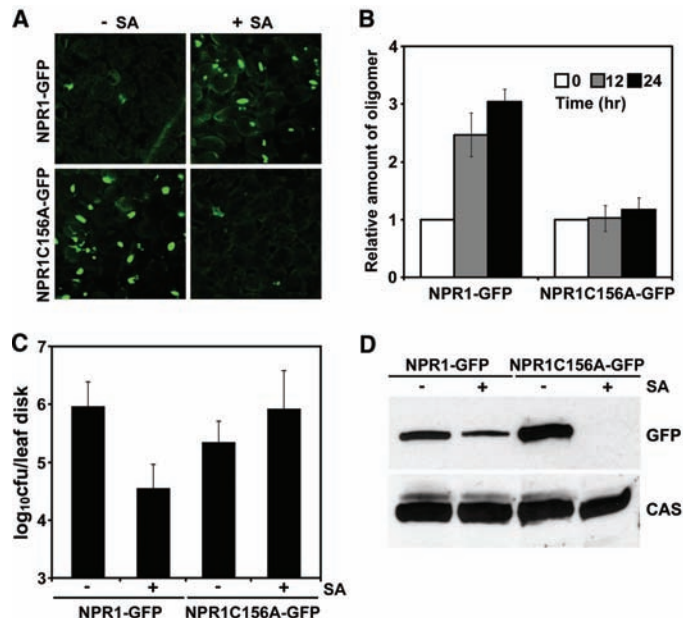


Fig. 3. S-nitrosylation of Cys¹⁵⁶ is essential for NPR1 protein homeostasis and SA-induced disease resistance. (A) SA treatment reduces the constitutive nuclear fluorescence of NPR1C156A-GFP. (B) The C156A mutation impairs NPR1 oligomer formation in response to SA. *35S::NPR1-GFP* and *35S::NPR1C156A-GFP* plants were treated with SA. The relative amount of NPR1 oligomer was determined by calculating densitometric ratios between induced and uninduced samples and normalized against total NPR1 protein. Error bars represent SD (*n* = 3 measurements). (C) SA-induced resistance is compromised in NPR1C156A plants. Error bars represent 95% confidence limits (*n* = 8 xxxxx). (D) SA treatment decreases NPR1C156A protein levels. *35S::NPR1-GFP* and *35S::NPR1C156A-GFP* plants were treated with (+) or without (–) SA for 48 hours. NPR1-GFP protein was detected with an antibody to GFP, and equal loading was verified with an antibody against constitutively expressed Ca²⁺-sensing receptor (CAS).



TRX-h5 with NPR1 suggests that it may be involved in catalysis of the NPR1 oligomer-to-monomer reaction during plant defense. We added recombinant TRX-h5 to cell lysates containing NPR1-GFP oligomer and showed that, compared to the control, the amount of NPR1-GFP monomer increased within 15 min of incubation (Fig. 4C).

TRX-h5 was required *in vivo* for SA-induced monomer release (Fig. 4D). Both *TRX-h3* and *TRX-h5* were required for full induction of *PR* genes (Fig. 4E). Additionally, in the *trx* mutants, NPR1-dependent systemic acquired resistance (SAR) against *Psm* ES4326, triggered after local inoculation of avirulent *Psm* ES4326/*avrRpt2*, was partially impaired (Fig. 4, F and G). Consistently, the TRX reductase knockout mutant *ntra* (20), which blocks the regeneration of cytosolic TRXs, showed a complete loss of SAR.

Our study provides a molecular mechanism to explain how cellular redox changes during pathogen challenge lead to transcriptional reprogramming and disease resistance (fig. S9). We propose that redox signals are conveyed through SNO and cytosolic TRXs, which directly catalyze the NPR1 oligomer-monomer exchange. Upon pathogen challenge, SA induces *TRX-5h* to catalyze the release of NPR1 monomer and possibly prevent oligomerization of some of the monomer. Induction also leads to S-nitrosylation of NPR1, which facilitates oligomerization to prevent protein depletion. SA-induced NPR1 oxidation and reduction may occur sequentially as the application of inducers of SAR results in tran-

sient oxidative and reductive fluctuations (3). To test this hypothesis, we treated plants with a combination of the translation inhibitor cycloheximide, the proteasome inhibitor MG115, and SA. In the absence of protein synthesis and degradation, SA-induced monomer accumulation was highest 12 hours after treatment. However, after 16 hours, NPR1 monomer re-oligomerized (fig. S10). The biological importance of controlling NPR1 homeostasis is demonstrated by the impaired immune responses of the *NPR1C156A* and *trx* mutants.

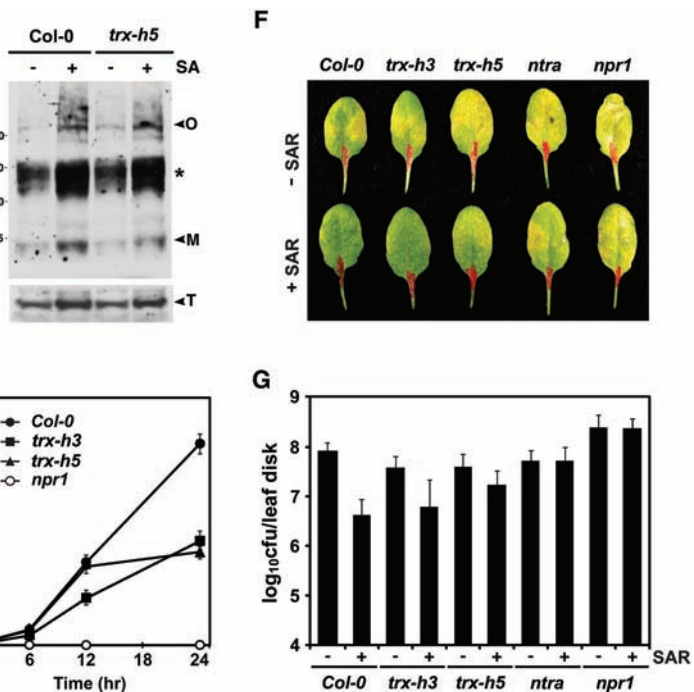
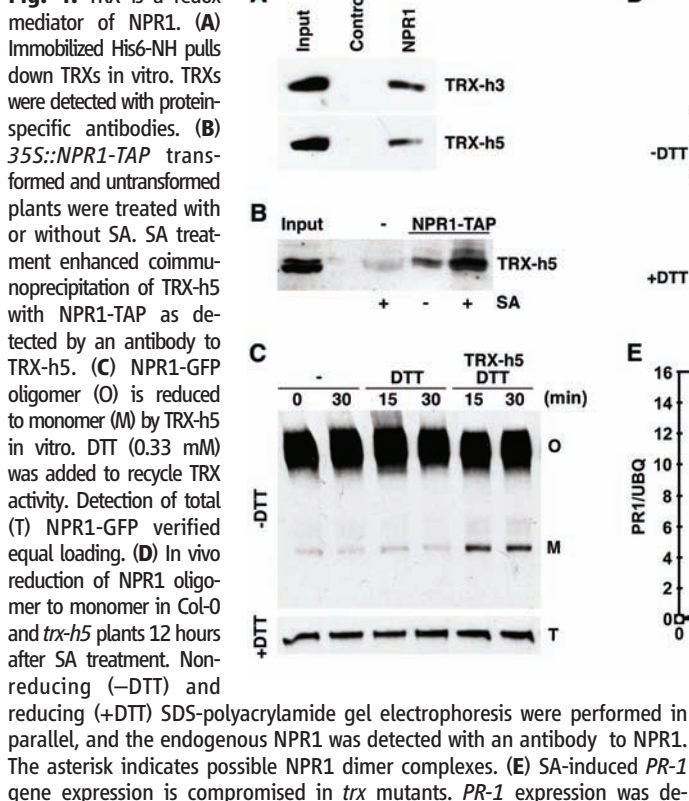
NO has long been proposed to be involved in responses to plant hormones, salt stress, ultraviolet light, and pathogens (21, 22). However, our knowledge of NO direct targets and its molecular effects on gene expression is limited. Recently, S-nitrosylation of *Arabidopsis* peroxiredoxin II E was shown to cause the accumulation of peroxynitrite (ONOO⁻) (23). Increased ONOO⁻ levels induced tyrosine nitration of proteins, which might activate the plant defense mechanism known as the hypersensitive response. Even though the *in vivo* concentration and subcellular localization of GSNO have yet to be determined, genetic studies with *Arabidopsis atgsnor* mutants indicated that GSNO functions as an endogenous signal in plant defense responses (7). The identification of NPR1 as a direct target of S-nitrosylation may explain the phenotype of the *atgsnor* mutants. In mammals, NO functions as an anti-inflammatory signal by S-nitrosylating IκB kinase β (IKKβ) (24), the catalytic subunit of IKK, required for activation of the tran-

scriptional immune regulator nuclear factor κB (NF-κB). S-nitrosylation of IKKβ inactivates IKK and retains NF-κB in the cytoplasm. This response is reminiscent of NPR1 oligomerization by S-nitrosylation, which prevents NPR1 from entering the nucleus (fig. S9). This suggests that redox-mediated transcription regulatory mechanisms are a common feature of immune responses in both plants and animals.

References and Notes

1. J. D. Jones, J. L. Dangl, *Nature* **444**, 323 (2006).
2. T. Nurnberger, F. Brunner, B. Kemmerling, L. Piater, *Immunol. Rev.* **198**, 249 (2004).
3. Z. Mou, W. Fan, X. Dong, *Cell* **113**, 935 (2003).
4. M. Kinkema, W. Fan, X. Dong, *Plant Cell* **12**, 2339 (2000).
5. K. J. Dietz, *Int. Rev. Cytol.* **228**, 141 (2003).
6. M. Delledonne, Y. Xia, R. Dixon, C. Lamb, *Nature* **394**, 585 (1998).
7. A. Feechan et al., *Proc. Natl. Acad. Sci. U.S.A.* **102**, 8054 (2005).
8. C. Lindermayr, G. Saalbach, J. Durner, *Plant Physiol.* **137**, 921 (2005).
9. J. S. Stamler et al., *Proc. Natl. Acad. Sci. U.S.A.* **89**, 444 (1992).
10. S. R. Jaffrey, H. Erdjument-Bromage, C. D. Ferris, P. Tempst, S. H. Snyder, *Nat. Cell Biol.* **3**, 193 (2001).
11. M. T. Forrester, M. W. Foster, J. S. Stamler, *J. Biol. Chem.* **282**, 13977 (2007).
12. D. T. Hess, A. Matsumoto, S. O. Kim, H. E. Marshall, J. S. Stamler, *Nat. Rev. Mol. Cell Biol.* **6**, 150 (2005).
13. D. R. Arnelo, J. S. Stamler, *Arch. Biochem. Biophys.* **318**, 279 (1995).
14. K. F. Ahmad et al., *Mol. Cell* **12**, 1551 (2003).
15. X. Li et al., *Cancer Res.* **59**, 5275 (1999).
16. G. Wang, N. H. Moniri, K. Ozawa, J. S. Stamler, Y. Daaka, *Proc. Natl. Acad. Sci. U.S.A.* **103**, 1295 (2006).
17. C. Laloi, D. Mestres-Ortega, Y. Marco, Y. Meyer, J. P. Reichheld, *Plant Physiol.* **134**, 1006 (2004).

Fig. 4. TRX is a redox mediator of NPR1.



termined by real-time PCR and normalized with *ubiquitin* (*UBQ*). Error bars represent SD. (F and G) Induction of SAR significantly decreased disease symptoms and *Psm* ES4326 growth in Col-0 plants but not in the *trx*, *ntra*, and *npr1-1* mutants. Error bars represent 95% confidence limits (*n* = 8 samples).

18. J.-P. Reichheld, D. Mestres-Ortega, C. Laloi, Y. Meyer, *Plant Physiol. Biochem.* **40**, 685 (2002).
19. K. Motohashi, A. Kondoh, M. T. Stumpp, T. Hisabori, *Proc. Natl. Acad. Sci. U.S.A.* **98**, 11224 (2001).
20. J. P. Reichheld *et al.*, *Plant Cell* **19**, 1851 (2007).
21. A. Besson-Bard, A. Pugin, D. Wendehenne, *Annu. Rev. Plant Biol.* **59**, 21 (2008).
22. S. Grun, C. Lindermayr, S. Sell, J. Durner, *J. Exp. Bot.* **57**, 507 (2006).
23. M. C. Romero-Puertas *et al.*, *Plant Cell* **19**, 4120 (2007).
24. N. L. Reynaert *et al.*, *Proc. Natl. Acad. Sci. U.S.A.* **101**, 8945 (2004).
25. We thank M. Delledonne, J. Stamler, K. Murase, A. Matsumoto, K. Kojima, and K. Ozawa for discussion; G. Loake and N. Spivey for the *atg5snor1-3* mutant and microarray data on TRXs, respectively; J. Yoo for technical assistance; Y. Meyer and Z. Pei for TRX-h3/TRX-h5 and CAS antibodies, respectively; and J. Stamler, J. Siedow, Z. Pei, and N. Spivey for critiquing the manuscript. Supported by a grant from NIH (1R01-GM69594) to X.D.

Supporting Online Material

www.sciencemag.org/cgi/content/full/1156970/DC1
Materials and Methods
Figs. S1 to S10
References

25 February 2008; accepted 2 July 2008

Published online 17 July 2008;

10.1126/science.1156970

Include this information when citing this paper.

A Global View of Gene Activity and Alternative Splicing by Deep Sequencing of the Human Transcriptome

Marc Sultan,^{1*} Marcel H. Schulz,^{2,3*} Hugues Richard,^{2*} Alon Magen,¹ Andreas Klingenhoff,⁴ Matthias Scherf,⁴ Martin Seifert,⁴ Tatjana Borodina,¹ Aleksey Soldatov,¹ Dmitri Parkhomchuk,¹ Dominic Schmidt,¹ Sean O'Keefe,² Stefan Haas,² Martin Vingron,² Hans Lehrach,¹ Marie-Laure Yaspo^{1†}

The functional complexity of the human transcriptome is not yet fully elucidated. We report a high-throughput sequence of the human transcriptome from a human embryonic kidney and a B cell line. We used shotgun sequencing of transcripts to generate randomly distributed reads. Of these, 50% mapped to unique genomic locations, of which 80% corresponded to known exons. We found that 66% of the polyadenylated transcriptome mapped to known genes and 34% to nonannotated genomic regions. On the basis of known transcripts, RNA-Seq can detect 25% more genes than can microarrays. A global survey of messenger RNA splicing events identified 94,241 splice junctions (4096 of which were previously unidentified) and showed that exon skipping is the most prevalent form of alternative splicing.

Global analysis of gene expression has mostly relied on RNA hybridization on high-density arrays (1–3), allowing the profiling of many tissues (4, 5) but detecting only specific sequences. Whole-genome tiling arrays theoretically allow the capture of much of the complexity of the transcriptome (6, 7), but they ignore splice-junction information and are associated with high costs and difficulties in data analysis. Arrays that specifically detect alternative splicing (AS) events (8, 9) have been hampered by issues of completeness and specificity.

Digital transcript-counting approaches overcome many of the inherent limitations of array-based systems and bypass problems inherent to analog measurements, including complex normalization procedures and limitations in detecting low-abundance transcripts. However, the expressed sequence tag (EST) approach, providing partial sequences of individual cDNA clones, is sensitive to cloning biases and has high

costs. Serial analysis of gene expression (10) and massively parallel signature sequencing (11) are also costly and cannot be used for splicing events.

The potential of RNA-Seq (short-read high-throughput sequencing) was first demonstrated by the polony multiplex analysis of gene expression, allowing the detection of 0.3 RNA copies per cell (12). Illumina-based RNA-Seq technology has recently been applied to yeast and *Arabidopsis thaliana* (13–15), providing transcriptome surveys at single-nucleotide resolution.

We present here a snapshot of the human transcriptome at base-pair resolution via RNA-Seq (16). Briefly, poly(A) RNA was extracted from human embryonic kidney (HEK) 293T and Ramos B cells and used to generate double-stranded cDNA using random hexamers as primers. The double-stranded DNA was sheared by sonication for preparing the sequencing libraries according to the Illumina protocol (16). Illumina deep sequencing was used to generate 27-base pair (bp) reads from replicate samples for each cell line. Reads were mapped to the human genome (hg18, National Center of Biotechnology Information build 36.1) using the Eland software, allowing up to two mismatches (16). Of the total reads, 50% matched to unique genomic locations, 16 to 18% showed multiple matches, and 25% had no match to the genome (Table 1 and table S1). 6000 reads from HEK were adenovirus or SV40 sequences,

reflecting the origin of this cell line. We mapped the unique reads to known genes based on both ENSEMBL (17) and RefSeq/EIDorado (Tables 1 and 2 and tables S1 and S2) (16): 80% of the unique reads mapped to known exons.

Digital expression levels were normalized (NE values) by taking into account the theoretical number of unique 27-mers (sequences that are 27 bases long) contained in each exon and the total number of reads generated in each experiment (table S2) (16).

To assess whether NE values were a reliable indicator of gene activity, we correlated these values with hypophosphorylated RNA polymerase II (PolIIa) occupancy, used as a landmark of transcription initiation (18). For HEK, we identified PolIIa islands by chromatin immunoprecipitation and sequencing (ChIP-Seq) (16). Figure 1 shows that the density of PolIIa reads correlates positively with gene expression levels. However, in contrast to a study reporting that 37% of the silent promoters contained PolII islands (19), we observed virtually no PolIIa near the promoters of silent genes. This apparent contradiction is most likely due to the higher sensitivity of RNA-Seq, detecting gene expression that would be scored silent with arrays (see below). The current model of the pre-recruitment of PolIIa at the promoter of silent genes (20) may be lacking sufficiently sensitive expression data. In Fig. 1, the peaks for low and moderately expressed genes exhibit a more pronounced shoulder than those for highly expressed genes. This might reflect the presence of a large preinitiation complex where PolIIa is parked upstream of the transcription start site (TSS) of the less active genes until activated, or the existence of alternative TSS. In clustering the reads specifying PolIIa-bound regions, we identified 9710 PolIIa-bound regions, of which 80% associated to known promoters (table S3) (16). Of the remaining 1936 PolIIa-bound regions, more than half were supported by Cap-analysis of gene expression (CAGE) tags (21), and 567 were either located within genes or less than 1 kb upstream of the next annotated transcript, representing putative alternative promoters.

In evaluating the dynamic range and sensitivity of RNA-Seq, we predicted the number of genes present within a cell type by applying a Poisson mixture statistical analysis on the number of reads mapped to genes (16, 22). We showed that the performances achieved for each sample corresponded to a gene identification score of 83 to 92% for HEK and 70 to

¹Department of Vertebrate Genomics, Max Planck Institute for Molecular Genetics, Ihnestrasse 73, 14195 Berlin, Germany. ²Department of Computational Molecular Biology, Max Planck Institute for Molecular Genetics, Ihnestrasse 73, 14195 Berlin, Germany. ³International Max Planck Research School for Computational Biology and Scientific Computing. ⁴Genomatix Software GmbH, Bayerstrasse 85a, 80335 Munich, Germany.

*These authors contributed equally to this work.

†To whom correspondence should be addressed. E-mail: yaspo@molgen.mpg.de